A R C H I V E S O F M E T A L L U R G Y A N D M A T E R I A L S
Volume 58 2013 Issue 1
DOI: 10.2478/v10172-012-0174-5

A. SMALCERZ*

ASPECTS OF APPLICATION OF INDUSTRIAL ROBOTS IN METALLURGICAL PROCESSES

ASPEKTY WYKORZYSTANIA ROBOTÓW PRZEMYSŁOWYCH W PROCESACH METALURGICZNYCH

Industrial robots are increasingly widely used in industrial metallurgical processes, their main aim being greater effectiveness of the process and higher precision of the tasks performed. The characteristic feature of numerous metallurgical processes, however, is the occurrence of strong electromagnetic fields. This paper presents the assessment of the accuracy of operation of an industrial robot in electromagnetic environment. The research encompassed the measurements of temperature of selected robot components and also the measurements of accuracy of the tasks performed. Additionally, some numerical simulations were carried out for determining the Joule losses produced in particular elements of the robot. The object of the research was an induction heater working with the industrial frequency. The numerical computations were performed by the code Flux 3D.
Keywords: induction heating, industrial robot, simulation, electromagnetic field, temperature field

Coraz szersze zastosowanie w procesach przemysłowych metalurgicznych znajdują roboty przemysłowe. Głównym celem stosowania robotów jest usprawnienie procesu oraz zwiększenie dokładności wykonywanych zadań. Jednak cechą charakterystyczną procesów metalurgicznych jest występowanie pola elektromagnetycznego o znacznym natężeniu. W publikacji została przeprowadzona ocena poprawności działania robota przemysłowego w środowisku elektromagnetycznym. Badania obejmowały pomiary temperatury elementów robota oraz dokładności wykonywania przez niego określonych zadań. Dodatkowo przeprowadzono symulacje numeryczne, w których wyznaczono moc wydzielaną w poszczególnych elementach robota. Obliczenia numeryczne wykonano przy użyciu programu komputerowego Flux 3D.

1. Introduction

One of the industrial branches where the devices used can be dangerous for employees as sources of electromagnetic field is electroheat treatment of materials. It is a sector of industry concerned with the transformations of electromagnetic field energy (generated by electric currents) into usable thermal energy together with the corresponding devices and their technical applications [1, 2, 3, 4]. One of the solutions eliminating the dangers of strong electromagnetic fields and improving the industrial process is using of different types of industrial robots and manipulators [5]. The most important features characterizing the performance of industrial robots follow [6]:

- Repeatability – a measure of precision with which the robot returns to the commanded point. It is a very important feature, especially in the situations where small tolerances are required.
- Accuracy – the measure of error showing how closely the robot can reach a particular point in the working space.
- Reliability – one of the most important features of the robot. It is the reliability that may in some cases stop the operation of the whole production plant.

The drawback of this solution is a possible disturbance of the robot operation by a strong magnetic field on one hand and heating of the robot or manipulator components on the other hand [7]. So the main goal of the investigations is a determination of Joule losses released in the metallic elements of the robot and consequent evaluation of its on induction heater.

2. Description of the studied object

Obtaining a strong electromagnetic field in the laboratory conditions was a serious problem, and it was solved by using a two-layer cylindrical induction heater working with frequency $f = 50$ Hz (see Fig. 1).

* SILESIAN UNIVERSITY OF TECHNOLOGY, DEPARTMENT OF MATERIAL SCIENCE AND METALLURGY, 40-019 KATOWICE, 8 KRASIŃSKIEGO STR., POLAND

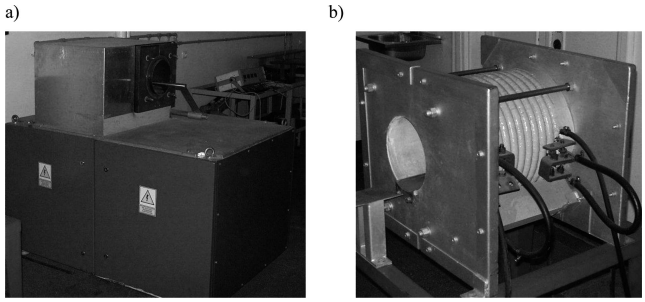

Fig. 1. Induction heater a) device with shield, b) inductor without shield

Figures 2 and 3 and Table 1 present the basic dimensions and power supply parameters of the device.

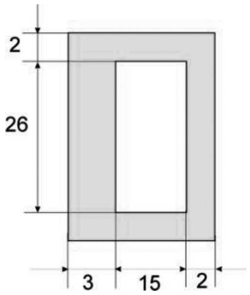

Fig. 2. Dimensions (in mm) of the inductor coil of the heater

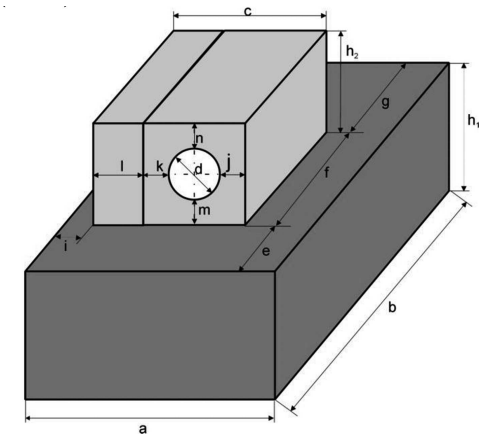

Fig. 3. Symbols of dimensions of induction heater

TABLE 1
Parameters and dimensions of induction heater

Parameter	Unit	Value							
Frequency	f, Hz	50							
Supply current	I, A	410							
Active power	P_n, kW	10							
Number of turns of winding	–	2×30 in two-layers							
Dimensions	mm	a	b	c	d	e	f	g	
		1100	1550	700	220	750	550	250	
		h_1	h_2	i	j	k	l	m	n
		900	500	50	90	90	300	190	90

Table 2 presents material properties of particular elements of the heating system.

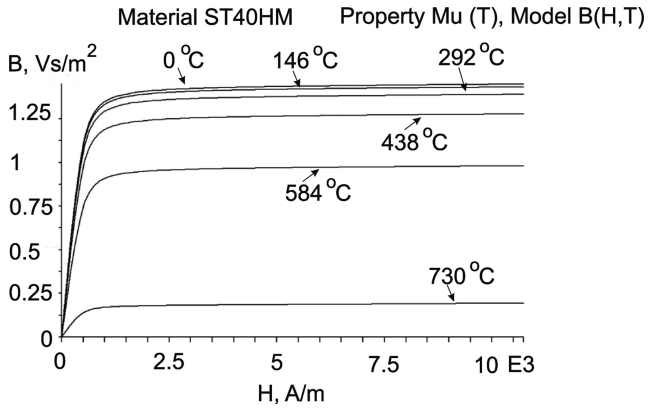

Fig. 4. Magnetization characteristic of the used material (steel 40HM) for different temperatures

A characteristic feature of the induction heater is the occurrence of a strong electromagnetic field. The high intensity zone (that may be dangerous for people) covers the area within about 0.8 m from the heater, while the hazardous zone covers the area within 1.8 m from the heater [9, 10]. The robot arm and its controller were placed in this zone, creating the environment for the described research.

The machine used for the experiment was a Kawasaki industrial robot with a pneumatic gripper and additional accessory (Fig. 5).

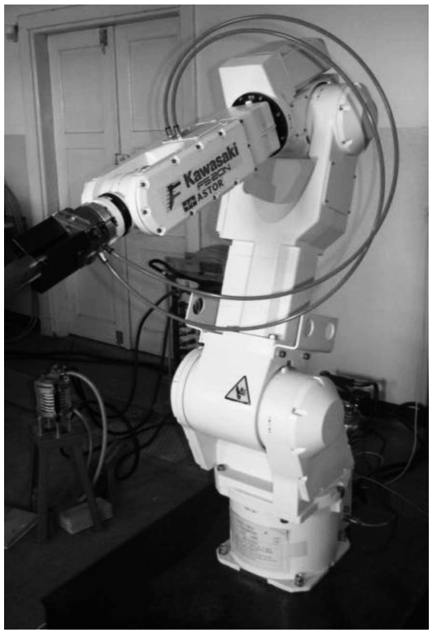

Fig. 5. Robot Kawasaki FS020NFD40 – max payload 20 kg

TABLE 2

Material properties

parameter	unit	approximation	quantity
work-piece (steel)			
resistivity	(Ωm)	linear $\rho = \rho_0 \cdot (1+aT)$	$\rho_0 = 1.6 \cdot 10^{-7}\Omega$m $\alpha = 6.18 \cdot 10^{-3}\mathrm{K}^{-1}$
relative magnetic permeability	(-)	scalar dependence $B(H)$, see Fig. 4	$B_S = 1.45$T $T_C = 750°$C
thermal conductivity	W/(m·K)	linear $\lambda = \lambda_0 \cdot (1+aT)$	$\lambda_0 = 42.4$ W/(m·K) $a = -0.00033$ (K)$^{-1}$
volumetric heat capacity	J/(m^{3}K)	special function [8]	$E = 5.83 \cdot 10^8$ J/m^3 $T_c = 750°$C $\sigma = 55°$C $V_0 = 3.7 \cdot 10^6$ J/(m^3 °C) $V_i = 5 \cdot 10^6$ J/(m^3 °C) $\tau = 500°$C
gripper fingers			
resistivity	(Ωm)	–	$\rho_0 = 1.7857 \times 10^{-8}\Omega$m
relative magnetic permeability	(-)	scalar dependence $B(H)$, see Fig. 4	$B_S = 1.45$T $T_C = 750°$C
thermal conductivity	W/(m·K)	linear $\lambda = \lambda_0 \cdot (1+aT)$	$\lambda_0 = 42.4$ W/(m·K) $a = -0.00033$ (K)$^{-1}$
volumetric heat capacity	J/(m^{3}K)	special function	$E = 5.83 \cdot 10^8$ J/m^3 $T_c = 750°$C $\sigma = 55°$C $V_0 = 3.7 \cdot 10^6$ J/(m^3 °C) $V_i = 5 \cdot 10^6$ J/(m^3 °C) $\tau = 500°$C
robot TCP, gripper			
resistivity	(Ωm)	–	$\rho_0 = 7.30 \cdot 10^{-7}\Omega$m
relative magnetic permeability	(-)	–	1
thermal conductivity,	W/(m·K)	linear $\lambda = \lambda_0 \cdot (1+aT)$	$\lambda_0 = 14.43$ W/(m·K) $a = 0.00108$ (K)$^{-1}$
volumetric heat capacity	J/(m^{3}K)	linear $\rho c = \rho c_0 \cdot (1+aT)$	$\rho c_0 = 3.84 \cdot 10^8$ J/(m^{3}K) $a = 0.000194$ (K)$^{-1}$
adapter			
resistivity	(Ωm)	linear $\rho = \rho_0 \cdot (1+aT)$	$\rho_0 = 0.265 \cdot 10^{-7}\Omega$m $\alpha = 0.004$ (K)$^{-1}$
relative magnetic permeability	(-)	–	1
thermal conductivity,	W/(m·K)	–	235
volumetric heat capacity	J/(m^{3}K)	–	$2.53 \cdot 10^6$

Note: α is the temperature coefficient of resistance, B_S is the saturation magnetic flux density and T_C is the Curie temperature.

3. Numerical model

To solve the eddy-current problems in three-dimensional systems, the model $\boldsymbol{T}\Phi - \Phi/\Phi_r$ was used. It combines the electric vector potential $\boldsymbol{T}$ and scalar magnetic potential Φ for conductive areas (both magnetic and non-magnetic) with Φ formulated for non-conductive magnetic areas and reduced scalar magnetic potential Φ_r for non-conductive and non-magnetic areas [8, 11].

The electric vector potential is defined by the formula

$$\boldsymbol{J} = \operatorname{curl} \boldsymbol{T} \tag{1}$$

The scalar magnetic potential Φ is described by the dependence

$$\boldsymbol{H} = \boldsymbol{T} - \operatorname{grad} \Phi \tag{2}$$

The above dependences lead to the equations which take the following form for harmonic quantities:

– for conductive areas

$$\operatorname{rot}\left(\frac{1}{\gamma}\operatorname{rot}\underline{T}\right) - \operatorname{grad}\left(\frac{1}{\gamma}\operatorname{div}\underline{T}\right) + \mathrm{j}\mu\omega(\underline{T} - \operatorname{grad}\underline{\Phi}) = 0 \tag{3}$$

$$\operatorname{div}[\mu(\underline{T} - \operatorname{grad}\underline{\Phi})] = 0 \tag{4}$$

where

$\operatorname{grad}(\frac{1}{\gamma}\operatorname{div}\underline{T})$ represents an expression referring to the boundary condition $\operatorname{div}\underline{\boldsymbol{T}} = 0$,

– for non-conductive areas such as magnetic areas (e.g., gripper fingers)

$$\operatorname{div}[\mu(-\operatorname{grad}\underline{\Phi})] = 0 \tag{5}$$

while for the non-magnetic areas

$$\mathrm{div}\,[\mu_0\,(-\mathrm{grad}\underline{\Phi}_r + \underline{H_0})] = 0. \tag{6}$$

The analysis of the temperature field was carried out by means of the classic Fourier-Kirchhoff equation taking the following form [8, 11]

$$\nabla \cdot (-\lambda \nabla T) + \rho c \frac{\partial T}{\partial \mathrm{t}} = q \tag{7}$$

where T is the temperature, λ denotes the thermal conductivity and q stands for the volumetric power density.

The complete mathematical model requires the initial and boundary conditions to be specified. The boundary condition described by (8) combines the radiation and convection models of heat dissipation

$$-\lambda \frac{\partial T}{\partial n} = \alpha(T - T_{0\mathrm{c}}) + \varepsilon\,\sigma(T^4 - T_{0\mathrm{r}}^4) \tag{8}$$

where α is the convection coefficient, ε denotes the emissivity and σ stands for the Stephan-Boltzmann constant, $\mathrm{T_{0c}}$ ambient temperature, $\mathrm{T_{0r}}$ temperature of radiation surface.

All numerical calculations, both for electromagnetic and temperature fields, were performed by program Flux 3D. A simplified diagram of these calculations is presented in Fig. 6.

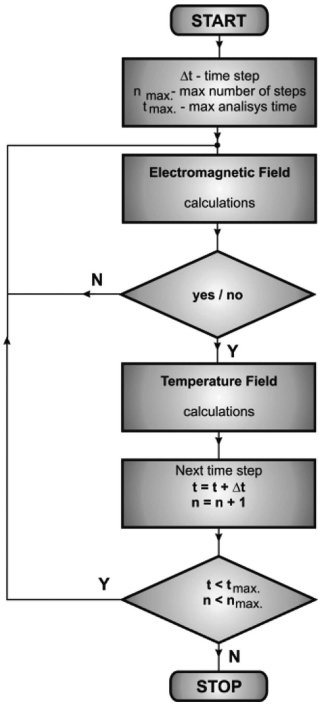

Fig. 6. General calculation model of the coupled analysis of electromagnetic and temperature fields

Figure 7 presents the arrangement used for the numerical modeling. It consists of the induction heater – workpiece (red), inductor (cyan) – and the following elements of the robot – gripper fingers (blue), pneumatic gripper (light blue), adapter (violet) and TCP (yellow).

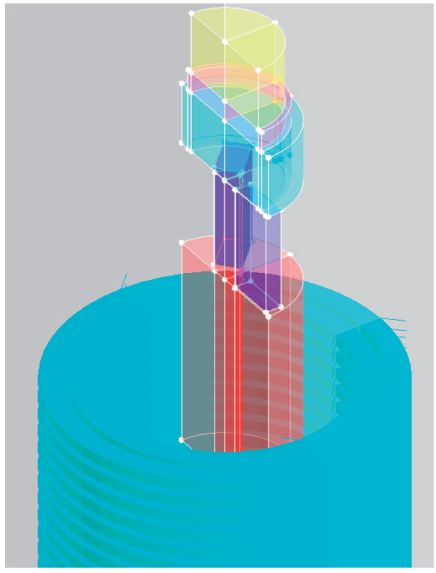

Fig. 7. Calculation model

4. Experimental procedures

During the experiment the performance of the robot was evaluated (repeatability, accuracy and reliability), and also the temperature growth of the working elements of the robot arm was measured.

The analysis involved the robot executing a specific program consisting of five cycles of the following actions performed in the given sequence:

- Taking the workpiece.
- Placing the workpiece in the heater.
- Three-minute heating (holding the workpiece in the running heater).
- Removing the workpiece.

During each cycle, the measurements of the positioning accuracy of the robot were realized in three characteristic positions:

1 – point of taking the workpiece (Fig. 8a),

2 – point of placing the workpiece into the heater (Fig. 8b),

3 – point of putting the workpiece back (Fig. 8c).

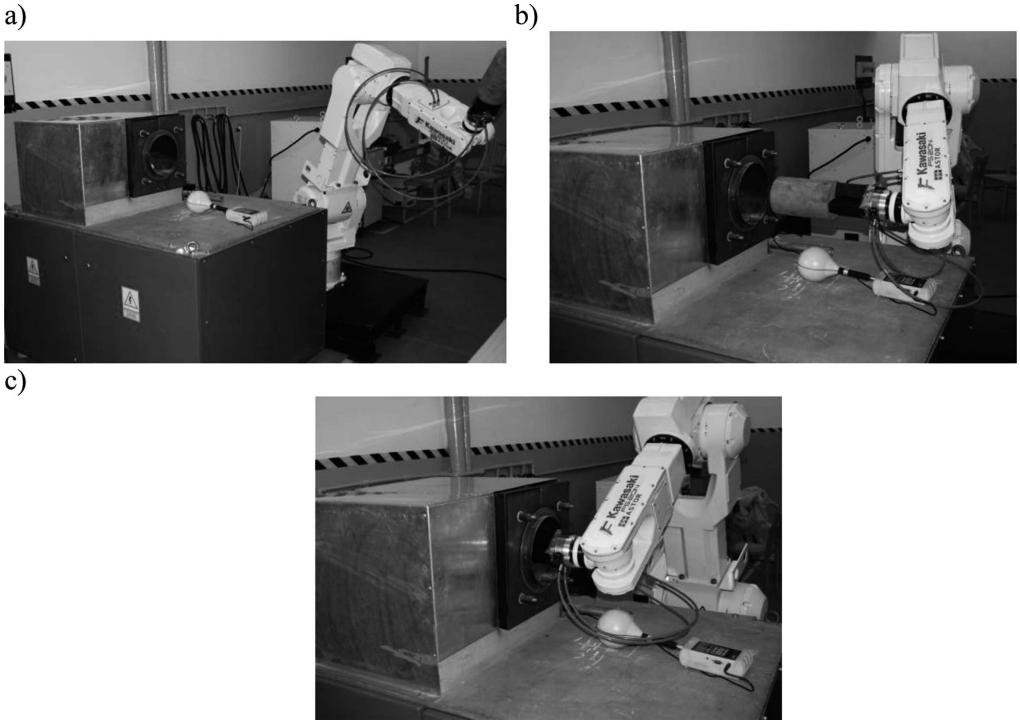

Fig. 8. Characteristic points of the robot operation, a) Point 1, b) Point 2, c) Point 3

5. Results and discussion

The aim of the experiment was to measure the temperature of the industrial robot arm, and particularly the temperature of the gripper (during the loading, heating and removing the workpiece), and to evaluate the accuracy and repeatability of the actions performed. The two last measurements were taken with a slide caliper. At this precision level no errors were found. The robot controller did not display any unusual behavior during the operation, either.

The temperature measurements were carried out with a pyrometer while the general temperature distribution measured by a thermocamera (Fig. 9) is presented in Fig. 10. This figure shows the robot gripper temperature distribution for selected moments of heating the workpiece. After the workpiece was taken by the gripper (point 1, Fig. 8a), the robot, as programmed, loaded the work-piece into the working heater. The workpiece remained in the inductor for three minutes and was heated (point 2 Fig. 8b). Picture 1 (in Fig. 10a) shows the temperature distribution for the elements of the robot, particularly for the gripper and the adapter, during the heating. After this time the workpiece was removed from the heater by the robot (point 3, Fig. 8c). The temperature distributions in the elements of the robot and workpiece at this stage are shown in picture 2 (Fig. 10b). Then, after 20 seconds the robot returned to point 2 (Fig. 8a). The program performed 5 identical cycles. Picture 3 (Fig. 10c) presents the temperature distribution after the last, that is, the fifth cycle.

The only undesirable side-effect of the robot operation under the influence of the electromagnetic field was that its elements heated. In the experiment described in the text the gripper fingers became the hottest, while the other parts were not heated to such a level. The maximum temperature of the gripper fingers was 70°C; the adapter did not reach the temperature exceeding 45°C, and the TCP was heated to about 35°C.

Fig. 9. Thermovision camera – Infrared Solution

The numerical simulations of the whole process of heating the workpiece were conducted, too. During the calculations the temperature of the elements and amount of the generated Joule losses were controlled. Table 3 presents the results of the analysis.

TABLE 3
Joule losses generated in the particular elements

Type of workpiece	P, W (workpiece)	P, W (fingers)	P, W (gripper)	P, W (adapter)	P, W (TCP)
magnetic steel	3275.5	15.7	181	139.4	8.2
Non-magnetic steel	1930.2	8.8	131.8	80	5.1
Aluminum	2273.3	5.2	111.2	69.5	4.4

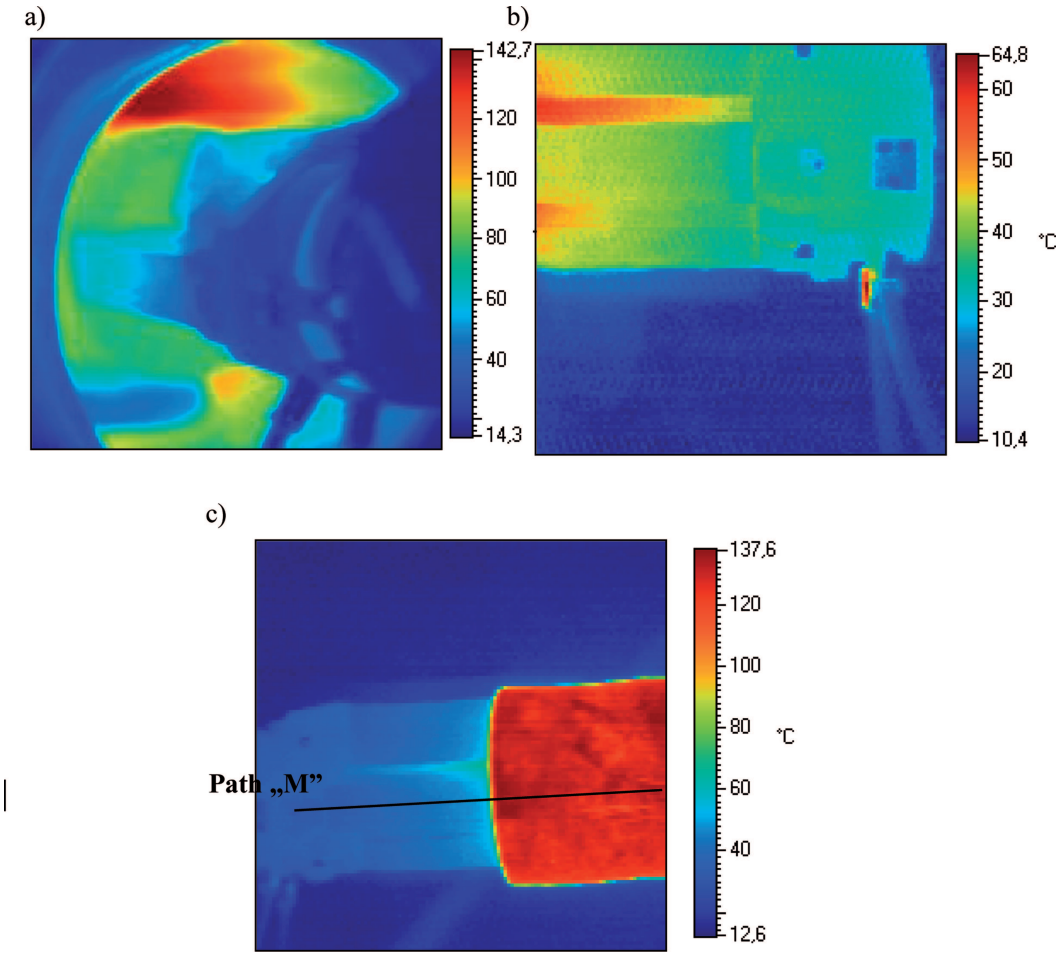

Fig. 10. Temperature distributions in the elements of the robot at the particular steps of the heating process: a) Picture 1. Temperature of gripper and adapter – 150 second after the workpiece was placed into the heater (point 2), b) Picture 2. Temperature of gripper and adapter – after removing the workpiece (point 3), c) Picture 3. Temperature of workpiece and gripper – end of the fifth cycle (point 1)

In the created computer model, heat transfer by conduction occurs between particular elements of the system. A simplification was made for the model that there is no physical contact between the robot gripper and the workpiece, while in reality, there is a point contact between them; however, taking this into account in the model would significantly increase the number of nodes and would lengthen the computation time. Figure 11 presents the temperature distribution (after the fifth cycle) obtained by the numerical calculations and Fig. 12 the distribution of temperature along the paths M and S (see Fig. 10 and 11).

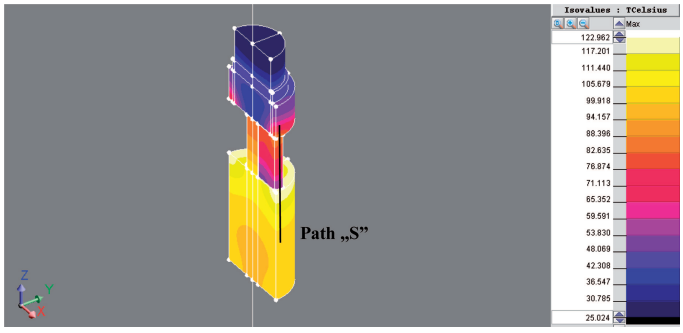

Fig. 11. Temperature distribution – numerical simulation

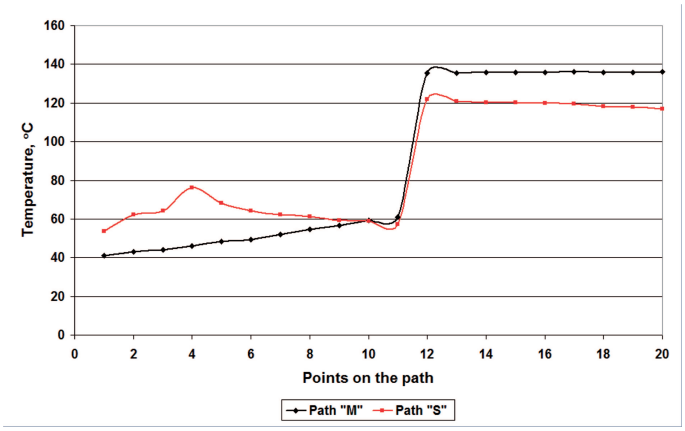

Fig. 12. Temperature distribution along two paths

6. Conclusions

The experiment consisted in placing the elements of the industrial robot into a strong magnetic field of the strength exceeding 2000 A/m for four minutes in each cycle. The following conclusions were reached:

- The magnetic field did not affect the accuracy of the tasks performed.

- The magnetic field did not influence the repeatability of the actions performed by the robot.
- During the experiment and research conducted for the mains-frequency heater, the robot carried out all the tasks as programmed (it worked reliably). During further operations no problems were encountered connected with the actions performed according to the program.
- The elements of the robot heated up under the influence of the magnetic field. The maximum temperature of the gripper fingers reached 70°C, although the exposure time was very short (altogether about 20 minutes) and a relatively low power heater was used taking into account industrial conditions and the chosen frequency. However, it should be remembered that during the experiment the fingers were inside the heater the entire time (similarly as the workpiece), which is not always necessary, (for example, when the robot will place the workpiece inside the heater and leave it there, and then remove it after it has been heated). This will reduce the temperature growth of the robot elements under the influence of the magnetic field and through thermal conduction (shorter time of contact with the work-piece). With each cycle the temperature of the elements grew, while the temperature gradients decreased significantly. In order to reduce the temperature growth, some specific materials can be used to cover the elements of the robot arm and insulate them from the heated elements.
- The temperature distributions obtained by measurements are strongly consistent with those obtained by the numerical simulations. Significant differences can only be noticed for the gripper fingers, which results from the simplification made for the computer model (no contact between the gripper and the work-piece).

Acknowledgements

This paper was supported by the Polish Ministry of Science and Higher Education under research project number N N508 479438.

Received: 10 February 2012.

REFERENCES

[1] A. B l a c h a, P. K o s c i e l n i a k, M. S i t a r z, J. S z u b e r, J. Z a k, Pedot brushes electrochemically synthesized on thienyl-modified glassy carbon surfaces, Electrochimica Acta **62**, 441-446 (2012).

[2] J. Ł a b a j, G. S i w i e c, B. O l e k s i a k, Surface tension of expanded slag from steel manufacturing in electrical furnace, Metalurgija **50** (3), 209-211 (2011).

[3] Cz. S a j d a k, S. G o l a k, A. K u r e k, Electromagnetic stirring of liquid ingot core in the process of continuous casting of steel, Przeglad Elektrotechniczny **83**, 67-70 (2007).

[4] J. B a r g l i k, Induction heating in technological processes – selected examples. Przeglad Elektrotechniczny **5** , 294-297 (2010).

[5] J. B a r g l i k, A. K u r e k, R. P r z y ł u c k i, et al., Change of electromagnetics field distribution around high and medium frequency heaters due to presence of industrial robots, Acta Technica **57**, 61-73 (2012).

[6] R. Z d a n o w i c z, Robotyzacja procesów technologicznych, Wydawnictwo Politechniki Śląskiej, Gliwice (2002).

[7] A. S m a l c e r z, R. P r z y l u c k i, Electromagnetic field analysis of inductor – robot – work-piece system, Metalurgija **52** (2), 223-226 (2013).

[8] FLUX3D 10.2 User's guide. Cedrat, Grenoble (2009).

[9] Directive 2004/40/EC of the European Parliament and of the Council of on the minimum health and safety requirements regarding the exposure of workers to the risks arising from physical agents (electromagnetic fields) (18th individual Directive within the meaning of Article 16(1) of Directive 89/391/EEC).

[10] Rozporządzenie Ministra Ochrony Środowiska z dnia 30 października 2003 r. w sprawie dopuszczalnych poziomów pól elektromagnetycznych w środowisku oraz sposobów sprawdzania dotrzymania tych poziomów. Dz. U. Nr 192, poz. 1883, (2003).

[11] M. N i k l e w i c z, A. S m a l c e r z, A. K u r e k, Estimation of system geometry and inductor frequency importance in induction hardening process of gears, Przeglad Elektrotechniczny **84** (11), 219-224 (2008).